Extended X-ray Absorption Fine Structure Analysis of Arsenite and Arsenate Adsorption on Maghemite

GUILLAUME MORIN,*,[†]
GEORGES ONA-NGUEMA,[†]
YUHENG WANG,[†] NICOLAS MENGUY,[†]
FARID JUILLOT,[†] OLIVIER PROUX,[‡]
FRANÇOIS GUYOT,[†] GEORGES CALAS,[†] AND
GORDON E. BROWN JR.[§,⊥]

Institut de Minéralogie et de Physique des Milieux Condensés (IMPMC), UMR 7590, CNRS, Université Paris 6, Université Paris 7, IPGP, 140, rue de Lourmel, 75015 Paris, France, European Synchrotron Radiation Facility (ESRF), Grenoble, France, Surface & Aqueous Geochemistry Group, Department of Geological and Environmental Sciences, Stanford University, Stanford, California 94305-2115, USA, and Stanford Synchrotron Radiation Laboratory, SLAC, 2575 Sand Hill Road, MS 69, Menlo Park, California 94025, USA

Arsenic sorption onto maghemite potentially contributes to arsenic retention in magnetite-based arsenic removal processes because maghemite is the most common oxidation product of magnetite and may form a coating on magnetite surfaces. Such a sorption reaction could also favor arsenic immobilization at redox boundaries in groundwaters. The nature of arsenic adsorption complexes on maghemite particles, at near-neutral pH under anoxic conditions, was investigated using X-ray absorption fine structure (XAFS) spectroscopy at the As K-edge. X-ray absorption near edge structure spectra indicate that As(III) does not oxidize after 24 h in any of the sorption experiments, as already observed in previous studies of As(III) sorption on ferric (oxyhydr)oxides under anoxic conditions. The absence of oxygen in our sorption experiments also limited Fenton oxidation of As(III). Extended XAFS (EXAFS) results indicate that both As(III) and As(V) form inner-sphere complexes on the surface of maghemite, under high surface coverage conditions (~0.6 to 1.0 monolayer), with distinctly different sorption complexes for As(III) and As(V). For As(V), the EXAFS-derived As−Fe distance (~3.35 ± 0.03 Å) indicates the predominance of single binuclear bidentate double-corner complexes (^2C). For As(III), the distribution of the As−Fe distance suggests a coexistence of various types of surface complexes characterized by As−Fe distances of ~2.90 (±0.03) Å and ~3.45 (±0.03) Å. This distribution can be interpreted as being due to a dominant contribution from bidentate binuclear double-corner complexes (^2C), with additional contributions from bidentate mononuclear edge-sharing (^2E) complexes and monodentate mononuclear corner-sharing complexes (^1V). The present results yield useful

* Corresponding author e-mail: guillaume.morin@impmc.jussieu.fr.
† Institut de Minéralogie et de Physique des Milieux Condensés.
‡ European Synchrotron Radiation Facility.
§ Stanford University.
⊥ Stanford Synchrotron Radiation Laboratory.

constraints on As(V) and As(III) adsorption on high surface-area powdered maghemite, which may help in modeling the behavior of arsenic at the maghemite−water interface.

Introduction

Important health issues result from arsenic levels in major groundwater resources above the recommended WHO concentration (10 μg L^{-1}) [e.g., ref *1*]. A recently proposed water treatment process for arsenic is based on magnetic separation and relies on arsenic sorption onto nanomagnetite particles (Fe$_3$O$_4$) (*2*). Small particles of magnetite (<100 nm) are known to rapidly oxidize to maghemite (γ-Fe$_2$O$_3$) in water suspensions equilibrated with the atmosphere, resulting in an oxidized surface layer and/or a nonstoichiometric composition (*3*, *4*). Consequently, the arsenic sorption reaction involved in such a water treatment process may involve surfaces of maghemite rather than of magnetite, unless special precautions are taken to prevent iron oxidation by O$_2$ dissolved in water. However, the ability to separate wholly or partially oxidized magnetite particles should not be significantly affected by this surface oxidation reaction because the bulk saturation magnetization of maghemite (76 emu g^{-1}) is only slightly lower that that of magnetite (92 emu g^{-1}; see, for example, ref *5*. and references therein). In addition to the potential role of this adsorption reaction in removal of arsenic from contaminated water by magnetic separation, arsenic sorption onto maghemite surfaces may favor the retention of arsenic at oxic-anoxic boundaries in groundwater after oxidation of biogenic magnetite (*6*).

In the present study, we investigated the reactivity of As(III) and As(V) with respect to fine particles of maghemite using X-ray absorption fine structure spectroscopy (XAFS). Such data are helpful in modeling sorption reactions as recently shown by Stachowicz et al. (*7*) in the case of As(III) and As(V) adsorption on goethite. We show that As(III) surface complexes differ from those of As(V), which is consistent with previous extended XAFS (EXAFS) findings for As(III) and As(V) sorption onto ferric (oxyhydr)oxides (*8*, *9*).

Experimental Section

Maghemite Samples. Two types of maghemite (γ-Fe$_2$O$_3$) were used in the present study: Alfa Aesar maghemite (ref No. J09M09) and a maghemite prepared at room temperature by complete oxidation by hydrogen peroxide of a biogenic magnetite prepared via the reduction of lepidocrocite (γ-FeOOH) by the ATCC 8071 strain of the dissimilatory Fe-respiring bacterium *Shewanella putrefaciens* (*10*, *11*). The mineralogical purity of both maghemite samples was checked by X-ray powder diffraction (XRD) (see Figure S1 of the Supporting Information). Detailed analysis of satellites lines in the low angle region of the XRD powder patterns indicated that the Alfa Aesar maghemite displays vacancy ordering and is thus of the quadratic type (Q-Mh) (*12*). The maghemite prepared by oxidation of biogenic magnetite is cubic (C-Mh) with very weak and broad satellites lines. Mössbauer spectroscopy at 296 K (not shown) showed that both maghemite samples had hyperfine parameters close to those of natural fine-grained maghemite (*13*).

Transmission electron microscopy (TEM) micrographs of the C-Mh sample showed octahedrally shaped crystals of 20–40 nm diameter with dominant (111) facets (Figure 1a). The Q-Mh sample exhibits round-shaped crystals 30–50 nm in diameter (Figure 1b). These particle size values are consistent with mean crystallite dimensions (MCD) determined by Rietveld refinement of XRD patterns (that is, 30 ±
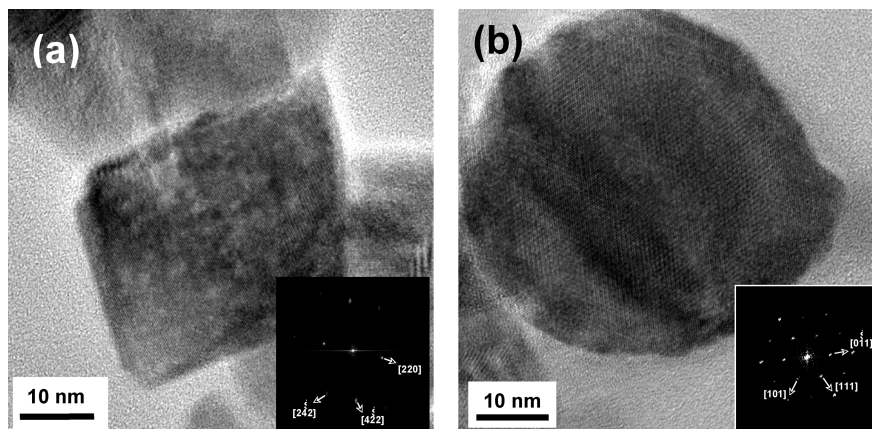
FIGURE 1. TEM images of the maghemite samples used for arsenic sorption experiments: (a) octahedral crystal of C-Mh obtained by oxidation of biogenic magnetite and its corresponding electron diffraction pattern along the [−113] zone axis; (b) crystal of commercial Q-Mh and its corresponding electron diffraction pattern along the [−111] zone axis.

2 nm and 43 ± 2 nm for the C-Mh and Q-Mh samples, respectively), indicating that most particles were single crystals. Specific surface area of C-Mh (40 ± 5 m^2 g^{-1}) is larger than that of the Q-Mh sample (30 ± 2 m^2 g^{-1}). These Brunauer−Emmett−Teller (BET) values agree (±5 m^2 g^{-1}) with specific areas calculated from MCD values (39 ± 2 and 27 ± 2 m^2 g^{-1} for C-Mh and Q-Mh, respectively).

Sorption Experiments. Sorption experiments were performed at an ionic strength of 0.1 N NaCl. Solutions of NaCl, NaOH, and sodium arsenate or sodium arsenite were prepared in O_2-free water obtained from Milli-Q water purged with N_2 (Alphagaz 1, Air–Liquide) at 80 °C. Adsorption experiments were carried out under a nitrogen atmosphere within a Jacomex glovebox. Suspensions of mineral sorbents were prepared by addition of 0.5 g of iron oxide in 38 mL of NaCl solution. A stock solution containing 66.8 mM As(III) was prepared by dissolving 0.868 g of $NaAsO_2$ (Sigma) in 100 mL of O_2-free water. A stock solution containing 66.8 mM As(V) was prepared by dissolving 2.084 g of $Na_2HAsO_4 \cdot 7H_2O$ (Sigma) in 100 mL of O_2-free water. After 1 mL of the stock solution of As(III) or As(V) was added to each iron oxide suspension, the pH was adjusted to 7.4 ± 0.2 with a 1 N NaOH solution. An appropriate volume of NaCl solution was then added to obtain a final volume of 40 mL and a final aresnic concentration of 1.67 mM. The flasks were incubated for 24 h in darkness at 25 °C and were agitated at 200 rpm. After 24 h of incubation, the pH values of the suspensions were measured with a glass combination pH electrode. The final pH value was within the 7.9–8.6 range for all experiments (Table 1). Solids were harvested by centrifugation (10 000g, 15 min) and vacuum-dried for six days in the glovebox prior to XAFS analysis. The concentration of arsenic in the solid sorption samples was measured by electron microprobe analysis (EMPA) at the Centre d'Analyses par Microsonde Electronique de Paris (Université Pierre et Marie Curie, Paris, France) using a SX50 CAMECA microprobe equipped with four Wavelength Dispersive spectrometers, operating at 20 kV and 40 nA and counting times of 10 s per element (As, Fe). Precision of the EMPA analysis after ZAF correction was estimated to be about 0.2 wt%. To determine surface coverage after the 24 h reaction, the supernatants were filtered through a 0.22 μm membrane and were acidified with HNO_3 in the glovebox to avoid precipitation of iron oxides that would cause a decrease in concentration of iron and arsenic in the solution. Arsenic concentrations were determined by atomic absorption spectrometry (AAS) on a Unicam 989 QZ spectrometer, with a standard deviation of ±10 μM.

XAFS Data Collection. XAFS data on the arsenic-treated Q-Mh and C-Mh samples were collected on bending magnet BM30B/FAME beamline at the European Synchrotron Ra-

diation Facility (ESRF, Grenoble, France) and on a wiggler beamline 10–2 at the Stanford Synchrotron Radiation Laboratory (SSRL). All data were collected on vacuum-dried samples at the arsenic K-edge (11 869 eV) using a Si(220) double-crystal monochromator in fluorescence detection mode, a 30 elements Ge array detector, and a Ge filter ($\ln(I_0/I_1)$ = 3) to attenuate elastic scattering and Fe fluorescence. Energy resolution was around 0.4–0.5 eV on both beamlines, with a spot size of 300 × 200 μm^2 on FAME (14) and 500 × 250 μm^2 on SSRL BL 10–2. Energy was calibrated using a double-transmission setup in which the arsenic K-edge spectrum of the samples and that of a reference sample were simultaneously recorded. The absorption maximum of the As(III)-edge was chosen at 11 871.3 eV. Using this energy calibration, the absorption maximum of As(V) is at 11 875 eV.

To limit As(III) oxidation in the X-ray beam (9, 15), all data were recorded at 10–15 K using modified Oxford liquid He cryostats on both beamlines. The samples were transferred via anoxic containers from the glovebox to the cryostat where they were placed in a He atmosphere. Between 8 and 15 EXAFS scans were accumulated for each sorption sample to obtain a reliable signal-to-noise ratio at k = 14.5 $Å^{-1}$. No reduction of As(V) was observed even after long-term beam exposure. However, each sample was automatically moved 1 mm between each EXAFS scan because we found that repeated scans on the same spot resulted in 7 ± 2% of As(III) being oxidized to As(V) after a 30 min EXAFS scan. This value is below the 10% detection limit of mixed species in EXAFS, for example, ref 16. Therefore, this small amount of As(V) occurring at the end of each EXAFS scan did not influence the results of our EXAFS fits on As(III) samples.

XANES and EXAFS Data Analysis. The oxidation state of arsenic was determined by linear least-squares fitting of the arsenic K-edge XANES data, using linear combinations of model compounds XANES spectra, following the procedure reported in ref 17. EXAFS data were extracted using the XAFS program (18) following the procedure detailed in ref 9. Fourier transforms (FT) of the $k^3\chi(k)$ EXAFS functions were obtained using a Kaiser−Bessel window within the 2.5–14.5 $Å^{-1}$ k-range with a Bessel weight of 2.5. For each EXAFS spectrum, first- and second-neighbor contributions to the FT were back-transformed together by Fourier filtering to yield partial EXAFS spectra of these two contributions. Least-squares fitting of the unfiltered and filtered $k^3\chi(k)$ functions were performed with the plane-wave formalism, using a Levenberg−Marquard minimization algorithm. Theoretical phase-shift and amplitude functions employed in this fitting procedure were calculated with the curved-wave formalism using the ab initio FEFF 8 code (19). As−O and As−Fe phase-shift and

TABLE 1. EXAFS Fit Parameters[a] and Sorption Data[b] for the As(III)- and As(V)-Treated Maghemites

sample (s.d.)	R (Å) (±0.03)	N (±0.5)	σ (Å) (±0.01)	ΔE_0 (eV) (±2)	CHI$_{FT}$	As$_{ad}$ (wt%) (±0.2)	As$_{ad}$ (%) (±1)	Γ (μmol m^{-2}) (±0.02)	Γ'	pH$_i$	pH$_f$
As(III)/C-Mh	1.77	3.0 O	0.07	16	(0.05)	0.8	93	3.07	0.8	7.5	8.6
	3.21	6.0 MS	–	–	0.02						
	2.90	0.3 Fe	0.10	–							
	3.45	0.7 Fe	–	–							
As(III)/Q-Mh	1.77	2.7 O	0.07	18	(0.09)	0.8	94	4.19	1.1	7.5	8.5
	3.22	6.0 MS	–	–	0.04						
	2.90	0.4 Fe	0.11	–							
	3.47	0.8 Fe	–	–							
As(V)/C-Mh	1.69	4.5 O	0.06	5	0.14	0.6	62	2.06	0.6	7.4	8.0
	3.09	12.0 MS	–	–	(0.17)						
	3.34	1.5 Fe	0.08	–							
As(V)/Q-Mh	1.69	3.7 O	0.05	6	0.07	0.6	67	2.99	0.8	7.2	7.9
	3.10	12.0 MS	–	–	(0.10)						
	3.35	1.1 Fe	0.08	–							

[a] R: interatomic distances; N: number of neighbors; σ: Debye–Waller factor; $\Delta E0$ (eV): difference between the Feff8-defined threshold energy and the experimentally determined threshold energy, in electron volts; CHI$_{FT}$: Goodness-of-fit (see text); the upper and lower values corresponds to the one and two As–Fe shells fits, respectively; the fitting parameters are only reported for the best solution, that is, with the lowest CHI$_{FT}$ value. During the fitting procedure, all parameter values indicated by (–) were linked to the parameter value placed above in the table. Standard deviations are estimated from the fit of the arsenolite and of the scorodite EXAFS spectra (not shown). The MS shell corresponds to As–O–O multiple-scattering paths within the AsO$_3$ pyramid and AsO$_4$ tetrahedron. Including this MS contribution improved the fits but did not change the results with respect to our standard deviation. [b] As$_{ad}$ (wt%): Concentration of arsenic in the solid phase measured by EMPA; As$_{ad}$ (%): Fraction of adsorbed arsenic in percentage of the initial arsenic concentration (1670 μM), calculated from the dissolved arsenic concentration in the supernatants measured by AAS; Γ: Surface coverage in μmol.m^{-2} calculated from the BET surface areas and the dissolved arsenic concentration in the supernatants measured by AAS; Γ': Surface coverage in (mole As)/(mole of surface sites), assuming an approximate site density of 2.31 sites nm^{-2}, that is, 3.7 μmol.m^{-2} (22–24).

amplitude functions were extracted from the tooeleite structure (20) and the scorodite structure (21), for As(III) and As(V), respectively.

The fit quality was estimated using a reduced χ^2 function of the following form:

$$\text{CHI}_{FT} = \frac{N_{ind}}{(N_{ind} - p)n} \sum_{i=1}^{n} (\|FT\|_{\exp_i} - \|FT\|_{\text{calc}_i})^2 \quad (1)$$

with $N_{ind} = (2\Delta k \Delta R)/\pi$ or the number of independent parameters, p the number of free fit parameters, n the number of data points fitted, $\|FT\|_{\exp}$ and $\|FT\|_{\text{calc}}$ the experimental and theoretical Fourier transform magnitude within the R-range 2.1–3.6 Å. This goodness-of-fit estimate was chosen because it was the most sensitive to the second-neighbor contributions to the EXAFS.

Results

Sorption Results. According to the concentration of dissolved arsenic measured in the supernatants after the 24 h reaction, the fraction of As(III) sorbed (93–94%) was higher than that of As(V) (62–67%) in all sorption experiments, indicating that As(III) sorbs more efficiently than As(V) at pH 8–8.5 on maghemite (Table 1). This result was confirmed by EMPA analyses of the solids, that is, 0.8 ± 0.2 wt% As and 0.6 ± 0.2 wt% As for As(III) and As(V) samples, respectively (Table 1). These EMPA values correspond to relative fractions of adsorbed arsenic of 80 ± 20% and 60 ± 20%, respectively. On the basis of the concentration of dissolved arsenic measured in the supernatants after the 24 h reaction and on the BET surface areas of the sorbents, the surface coverages were lower for the C-Mh sample (3.07 ± 0.02 and 2.06 ± 0.02 μmol m^{-2} for As(III) and As(V), respectively) than for the Q-Mh sample (4.19 ± 0.02 and 2.99 ± 0.02 μmol m^{-2} for As(III) and As(V), respectively). This difference can be related to the difference in surface area between the two maghemite

samples. Assuming an approximate site density of 2.31 nm^{-2} (22–24), the above values correspond to surface coverages of about 0.8 and 0.6 monolayers of As(III) and As(V), respectively, for the C-Mh sample. Arsenic surface coverage on the Q-Mh sample is higher, with about 1.1 and 0.8 monolayers of As(III) and As(V), respectively (Table 1).

Arsenic Oxidation State. Arsenic K-edge XANES spectra exhibit an absorption maximum at 11 871.3 eV for As(III)-sorbed samples and at 11 875.0 eV for As(V)-sorbed samples (Figure 2a). The As(V) content determined by linear least-squares fitting of the XANES data of As(III)-sorbed samples ranged between 0.05 and 1%, which falls below the detection limit of the method, which is 5% (17). Linear least-squares fitting indicated that As(V)-sorbed samples did not contain detectable As(III). As detailed in the Experimental Section, the fraction of As(III) oxidized under the beam during one EXAFS scan (7 ± 2%) was below the 10% detection limit of mixed species in EXAFS, for example, ref 16. Therefore, because the sample was moved between each EXAFS scan, this small amount of As(V) did not influenced the results of our EXAFS fits on As(III) samples.

Arsenite and Arsenate EXAFS Analysis. Arsenic K-edge unfiltered k^3-weighted EXAFS data of As(III)- and As(V)-sorbed maghemite samples and their FTs are displayed in Figures 2b and 2c. Table 1 lists the results of the fitting of the unfiltered $k^3\chi(k)$ EXAFS functions. First-neighbor contributions were fit with 3.7–4.5 oxygen atoms at 1.69 ± 0.03 Å and 2.7–3.1 oxygen atoms at 1.77 ± 0.03 Å in the As(V)/iron oxide and As(III)/iron oxide sorption samples, respectively (Table 1). These coordination number and distances correspond to the regular AsO$_4$ tetrahedron (21) and AsO$_3$ pyramid (20), respectively. In all samples, second-neighbor contributions to the EXAFS were fit using As–Fe pairs at various distances and a multiple-scattering (MS) contribution corresponding to the 12 or 6 As–O–O paths within the AsO$_4$ tetrahedron or AsO$_3$ pyramid, respectively (Table 1). The numbers of
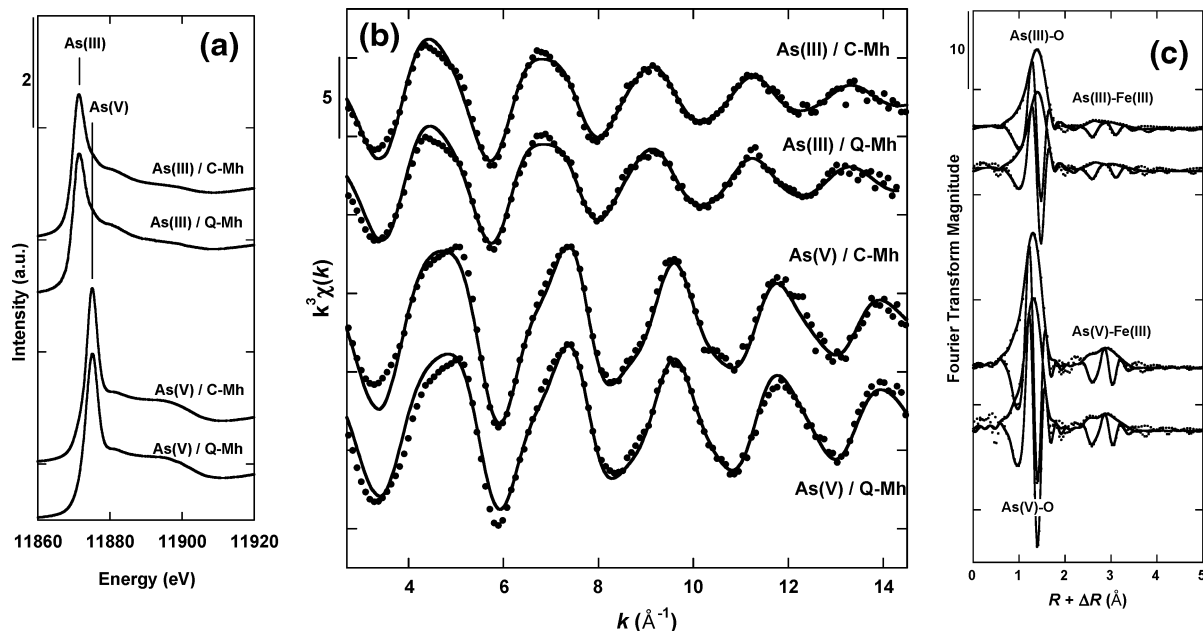
FIGURE 2. Arsenic K-edge XAFS data recorded at 10 K for As(III)- and As(V)-sorbed onto C-Mh and Q-Mh samples. (a) XANES data; (b) unfiltered k^3-weighted EXAFS data; (c) magnitude and imaginary part of the FT of the k^3-weighted $\chi(k)$ EXAFS. Results of the fit of the k^3-weighed EXAFS are reported with their corresponding FT (Table 1). Experimental and calculated curves are displayed as dashed and solid lines, respectively.
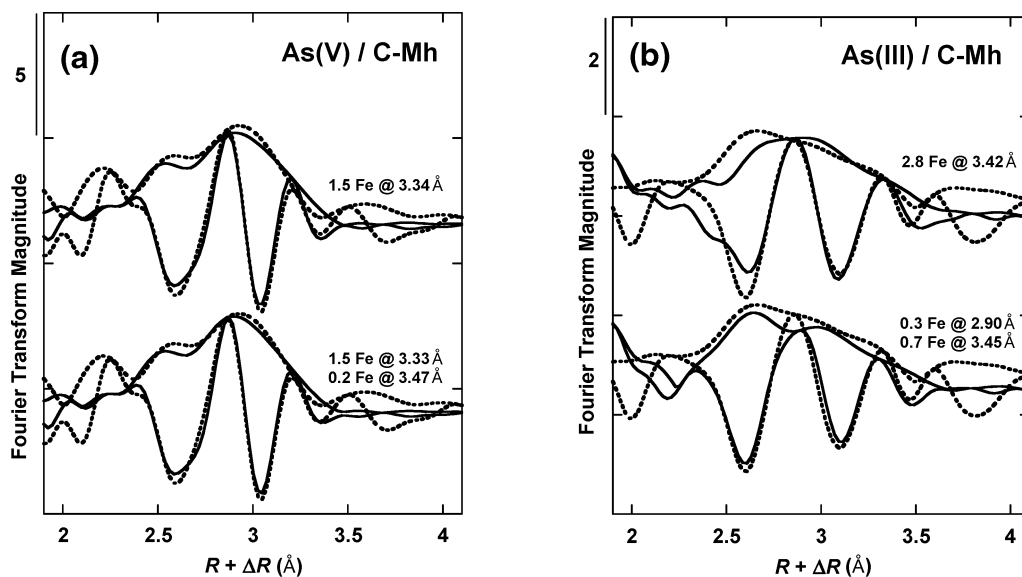

FIGURE 3. Details of the experimental and calculated FT obtained from the fit of the raw k^3-weighted EXAFS data of the As(III) and As(V) C-Mh sorption samples, including one or two As–Fe shells. Experimental and calculated curves are displayed as dashed and solid lines, respectively. (a) As(V)-treated samples; (b) As(III)-treated samples.

neighbors associated with these MS contributions were fixed at these expected values. The distances fitted for this MS contribution in our sorption samples range from 3.09 to 3.22 Å and thus agree with the corresponding distances in the structure of arsenolite (3.14 Å) and scorodite (3.05 Å), respectively. In all samples studied, the contribution of second neighbors (As–Fe shell) is weak with respect to that of first neighbors (As–O shell) (Figure 2c), supporting the occurrence of mononuclear arsenic surface complexes instead of (surface) precipitates. Separately fitting the second-neighbor contributions yields results similar to those obtained by fitting the unfiltered k^3-weighted EXAFS data. Discrepancies between the results obtained using these two fitting procedures fall within the estimated standard deviations determined by fitting the first- and second-neighbor contributions in the EXAFS spectra of both tooeleite

$(Fe_6(AsO_3)_4SO4(OH)_4 \cdot 4H_2O)$ and scorodite $[Fe(AsO_4) \cdot 2H_2O]$ (data not shown).

Arsenic(V) Samples. For both C-Mh and Q-Mh samples, the second-neighbor contributions in the EXAFS spectrum were satisfactorily fit by 1.5 Fe atoms at 3.35 ± 0.03 Å (Figures 2b, 2c, and 3a, Table 1). For both samples, addition of another Fe shell at a longer distance of ~3.5 Å did not improve the fit, and the CHI_{FT} value systematically increased when including this additional Fe shell (Table 1). A comparison of the two fits is displayed in Figure 3a for the C-Mh sample.

Arsenic(III) Samples. For both As(III)-treated maghemite samples, fitting the second-neighbor contribution using a single As–Fe shell at ~ 3.45 Å yielded discrepancies between calculated and experimental FTs, as illustrated for C-Mh samples in Figure 3b. Better fits were obtained when using two As–Fe shells (2.90 ± 0.03 and 3.45 ± 0.03 Å, or 3.35 ±

0.03 and 3.50 ± 0.03 Å), thus suggesting a distribution of As−Fe distances. Including three As−Fe shells at 2.90 ± 0.03, 3.35 ± 0.03, and 3.50 ± 0.03 Å yielded good fits but exceeded the number of allowed variable parameters, so this solution was not retained. The solution with two As−Fe shells at 2.90 and 3.45 Å was chosen because it yields the best CHI$_{FT}$ value (Table 1, Figure 3b).

Discussion

Arsenic Oxidation State. As(III) did not oxidize and As(V) did not reduce in any of the experiments. Thermodynamic data predict that the reduction of dissolved Fe(III) could be coupled with the oxidation of dissolved As(III) (*25*). However it is difficult to predict whether this reaction could occur for As(III) sorbed onto maghemite. Our XANES data indicate no observable change in arsenic oxidation state in any of the sorption samples within 24 h. This kinetic limitation is consistent with XANES results recently obtained for As(III) sorption onto ferric-oxyhydroxides, which showed that As(III) did not oxidize in the presence of ferrihydrite, goethite, or lepidocrocite even after 1 week of equilibration time under anoxic conditions (*9*). In contrast, the oxidation of As(III) is known to occur under oxic and slightly oxidizing (microaerophilic) conditions when Fenton reactions take place via reactive oxygen species (e.g., O_2^-, H_2O_2, or $^\bullet OH$) formed as intermediate species during the oxidation of Fe(II) by dissolved O_2 (*26*). We have recently confirmed, in the case of As(III)-sorption on hydrous ferric oxide, that is, two-line ferrihydrite, that As(III) can oxidize in the presence of sunlight under oxic conditions. This partial oxidation of As(III) is thought to be due to a Fenton reaction involving Fe(II) originating from photoreduction of Fe(III). This small amount of dissolved Fe(II) could indeed react with dissolved O_2 to form active radical species able to oxidize As(III) (*9*). Further studies are needed to evaluate the importance of Fenton oxidation of As(III) to As(V), especially in magnetite-based water treatment processes, in the presence of O_2.

Comparison between Arsenic Sorption on Maghemite and on Other Iron-oxides. The similarity between the As K-EXAFS results obtained for the C-Mh and Q-Mh samples studied suggests that the nature of the arsenic sorption complexes depend neither on the vacancy ordering nor on the surface coverage, within the range investigated (~0.6 to 1.0 monolayers). The crystallographic difference between the C-Mh and Q-Mh did not influence the nature of the arsenic sorption complexes. TEM observations indicate that maghemite particles in the C-Mh sample are mostly single crystals with octahedral shape displaying well developed (111) facets (Figure 1a); maghemite particles exhibit rounded shape in the Q-Mh sample (Figure 1b). The similarity between our As K-EXAFS results for these two maghemite samples suggests that this difference in crystal morphology does not influence the nature of the arsenic sorption complexes at the high surface coverage investigated. Full understanding of the geometry of arsenic surface complexes on maghemite would require knowledge of the structure of hydrated maghemite surfaces. In the absence of such data in the available literature, our EXAFS results can be compared with available data on arsenic surface complexes on other iron (oxyhydr)oxides.

Arsenite. Fitting of the second-neighbor contribution in the EXAFS spectra of the As(III)-sorption samples indicated a distribution of As−Fe distances within the 2.9–3.5 Å range. This distribution suggests that the hydrated surface of maghemite particles offers a wide variety of surface sites available for adsorption, which might be related to structural disorder at the crystal surfaces. Such disorder could be due to the preparation procedure, at least in the case of the C-Mh sample, which was obtained by rapid oxidation of biogenic magnetite at room temperature. The dominant As−Fe distance at 3.45 Å (Table 1, Figures 2 and 3) is slightly longer

than the bidentate binuclear corner-sharing surface complex (^2C), and is slightly shorter than that of a monodentate mononuclear corner-sharing surface complex (^1V), that is, 3.3–3.4 Å and 3.5 Å, repectively (*9*). This dominant As−Fe distance at 3.45 Å could be due to a mixture of contributions from both ^2C and ^1V complexes. The additional short As−Fe distance at 2.95 ± 0.03 Å can be interpreted as a bidentate mononuclear edge-sharing surface complex (^2E), similar to what has already been observed for As(III) adsorption onto hematite and ferrihydrite (*9*). Arsenite adsorbs in different modes on goethite and lepidocrocite (^2C and ^1V complexes only) (*9, 27*), as recently confirmed by DFT and CD modeling of sorption isotherms (*7*). Therefore, the present results on arsenite adsorption on maghemite confirm that the ^2E surface complex is characteristic of arsenite bonding to iron-(oxyhydr)oxide surfaces, by comparison with arsenate for which this ^2E surface complex is virtually absent (*16, 28–33*).

Arsenate. For arsenate, the As−Fe distance of 3.35 ± 0.03 Å is dominant in our samples (Table 1). This distance is similar to that reported by Manning et al. (*8*) (3.38 ± 0.06 Å) for arsenate sorption onto maghemite at very low coverage (0.012 monolayer). Although slightly longer than the distance of 3.30 ± 0.05 Å generally observed for arsenate adsorbed on iron-(oxyhydr)oxides (*16, 28–33*), the As−Fe distance of 3.35 ± 0.03 Å observed for maghemite can be interpreted as bidentate corner-sharing (^2C) surface complexes. Manning et al. (*8*) also found an additional Fe shell at 3.54 Å, which was interpreted as being due to a monodentate mononuclear corner-sharing (^1V) complex (*8, 16, 29–31, 33*). This component was negligible in our high coverage samples. The present results confirm that As(V) dominantly bonds to iron-(oxyhydr)oxide surfaces with characteristic As−Fe distance of 3.30–3.35 Å, consistent with bidentate corner-sharing (^2C) surface complexes, regardless of the iron oxide mineral considered, that is, maghemite (*8*), ferrihydrite (*16, 28, 29, 32*), lepidocrocite (*8, 34*), and goethite (*8, 30, 31*).

Conclusion

The present XAFS study provides evidence for the formation of arsenic inner-sphere complexes at the maghemite-water interface, with distinctly different sorption complexes for As(III) and As(V). As(V) bonds to the surface as single binuclear bidentate double-corner complexes (^2C). For As(III) the observed distribution of As-Fe distances can be interpreted as the coexistence of various types of surface complexes, including a dominant bidentate binuclear double-corner complexes (^2C), with additional contributions from bidentate mononuclear edge-sharing (^2E) complexes and monodentate mononuclear corner-sharing complexes (^1V).

These results may help in modeling the behavior of arsenic at the maghemite-water interface. However, our data doesn't preclude the possibility that a fraction of As(III) and/or As(V) might be adsorbed as outer-sphere complexes, which would have important environmental implications. Resonant anomalous x-ray reflectivity (RAXR) studies of arsenic sorption on iron oxides would be useful to investigate the possible existence of arsenic outer-sphere complexes on single-crystal maghemite samples, assuming suitable samples were available (*35*).

Acknowledgments

Supporting Information Available

XRD patterns of the two maghemite samples are displayed in Figure S1. This material is available free of charge via the Internet at http://pubs.acs.org.

Literature Cited

(1) Vaughan, D. J. Arsenic. *Elements* **2006**, *2*, 71–75.

(2) Yavuz, C. T.; Mayo, J. T.; Yu, W. W.; Prakash, A.; Falkner, J. C.; Yean, S.; Cong, L. L.; Shipley, H. J.; Kan, A.; Tomson, M.; Natelson, D.; Colvin, V. L. Low-field magnetic separation of monodisperse Fe_3O_4 nanocrystals. *Science* **2006**, *314*, 964–967.

(3) Ozdemir, O.; Dunlop, D. J.; Moskowitz, B. M. The effect of oxidation on the Verwey transition in magnetite. *Geophys. Res. Lett.* **1993**, *20*, 1671–1674.

(4) Moskowitz, B. M.; Frankel, R. B.; Bazylinski, D. A. Rock magnetic criteria for the detection of biogenic magnetite. *Earth Planet. Sci. Lett.* **1993**, *120*, 283–300.

(5) Millan, A.; Urtizberea, A.; Silva, N. J. O.; Palacio, F.; Amaral, V. S.; Snoeck, E.; Serin, V. Surface effects in maghemite nanoparticles. *J. Magn. Magn. Mater.* **2007**, *312*, L5–L9.

(6) Coker, V. S.; Gault, A. G.; Pearce, C. I.; vanderLaan, G.; Telling, N. D.; Charnock, J. M.; Polya, D. A.; Lloyd, J. R. XAS and XMCD Evidence for Species-Dependent Partitioning of Arsenic During Microbial Reduction of Ferrihydrite to Magnetite. *Environ. Sci. Technol.* **2006**, *40*, 7745–7750.

(7) Stachowicz, M.; Hiemstra, T.; van Riemsdijk, W. H. Surface speciation of As(III) and As(V) in relation to charge distribution. *J. Colloid Interface Sci.* **2006**, *302*, 62–75.

(8) Manning, B. A.; Hunt, M. L.; Amrhein, C.; Yarmoff, J. A. Arsenic(III) and arsenic(V) reactions with zerovalent iron corrosion products. *Environ. Sci. Technol.* **2002**, *36*, 5455–5461.

(9) Ona-Nguema, G.; Morin, G.; Juillot, F.; Calas, G.; Brown, G. E., Jr. EXAFS analysis of arsenite adsorption onto two-line ferrihydrite, hematite, goethite, and lepidocrocite. *Environ. Sci. Technol.* **2005**, *39*, 9147–9155.

(10) Ona-Nguema, G.; Abdelmoula, M.; Jorand, F.; Benali, O.; Géhin, A.; Block, J.-C.; Génin, J.-M. R. Iron(II, III) hydroxycarbonate green rust formation and stabilization from lepidocrocite bioreduction. *Environ. Sci. Technol.* **2002**, *36*, 16–20.

(11) Ona-Nguema, G.; Jorand, F.; Benali, O.; Abdelmoula, M.; Génin, J.-M. R.; Block, J.-C. Key role of the kinetics of γ-FeOOH bioreduction on the formation of Fe(II)-Fe(III) minerals. In *Proceedings of the International Conference on the Applications of the Mössbauer Effect (ICAME 2001). Hyperfine Interactions (C)*; Thomas MF, W. J., Gibb TC, Ed.; Dordrecht: Kluwer Academic Publishers: Oxford (UK), **2001**, *5*, 415-418.

(12) Shmakov, A. N.; Kryukova, G. N.; Tsybulya, S. V.; Chuvilin, A. L.; Solovyeva, L. P. Vacancy ordering in gamma-Fe_2O_3 — synchrotron x-ray-powder diffraction and high-resolution electron-microscopy studies. *J. Appl. Crystallogr.* **1995**, *28*, 141–145.

(13) Vandenberghe, R. E.; Barrero, C. A.; da Costa, G. M.; Van San, E.; De Grave, E. Mössbauer characterization of iron oxides and (oxy)hydroxides: the present state of the art. *Hyperfine Interact.* **2000**, *126*, 247–259.

(14) Proux, O.; Biquard, X.; Lahera, E.; Menthonnex, J.-J.; Prat, A.; Ulrich, O.; Soldo, Y.; Trévisson, P.; Kapoujyan, G.; Perroux, G.; Taunier, P.; Grand, D.; Jeantet, P.; Deleglise, M.; Roux, J.-P.; Hazemann, J. L. FAME: a new beamline for X-ray absorption investigations of very-diluted systems of environmental, material and biological interests. *Phys. Scr.* **2005**, *T115*, 970–973.

(15) Morin, G.; Guyot, F.; Lebrun, S.; Ona-Nguema, G.; Baranger, P.; Personne, J.-C.; Bonnefoy, V. Report: Role of microorganisms on oxidation state and trapping mechanisms of As by iron oxides; European Synchrotron Radiation Facility, **2004**.

(16) Cances, B.; Juillot, F.; Morin, G.; Laperche, V.; Alvarez, L.; Proux, O.; Hazemann, J. L., Jr.; Calas, G. XAS evidence of As(V) association with iron oxyhydroxides in a contaminated soil at a former arsenical pesticide processing plant. *Environ. Sci. Technol.* **2005**, *39*, 9398–9405.

(17) Morin, G.; Juillot, F.; Casiot, C.; Bruneel, O.; Personne, J. C.; Elbaz-Poulichet, F.; Leblanc, M.; Ildefonse, P.; Calas, G. Bacterial formation of tooeleite and mixed arsenic(III) or arsenic(V)−iron(III) gels in the Carnoules acid mine drainage, France. A XANES, XRD, and SEM study. *Environ. Sci. Technol.* **2003**, *37*, 1705–1712.

(18) Winterer, M. XAFS — A data analysis program for material science. *J. Phys. IV* **1997**, *7*, 243–244.

(19) Ankudinov, A. L.; Ravel, B.; Rehr, J. J.; Conradson, S. D. Real space multiple scattering calculation and interpretation of X-ray absorption near edge structure. *Phys. Rev. B* **1998**, *58*, 7565–7576.

(20) Morin, G.; Rousse, G.; Elkaim, E. Crystal structure of tooeleite, $Fe_6(AsO_3)_4SO_4(OH)_4 \cdot 4H_2O$, a new iron arsenite oxyhydroxysulfate mineral relevant to acid mine drainage. *Am. Mineral.* **2007**, *92*, 193–197.

(21) Hawthorne, F. C. The hydrogen positions in scorodite. *Acta Crystallogr.* **1976**, *B32*, 2891–2892.

(22) Dixit, S.; Hering, J. G. Comparison of arsenic(V) and arsenic(III) sorption onto iron oxide minerals: implications for arsenic mobility. *Environ. Sci. Technol.* **2003**, *37*, 4182–4189.

(23) Goldberg, S.; Johnston, C. T. Mechanisms of arsenic adsorption on amorphous oxides evaluated using macroscopic measurements, vibrational spectroscopy, and surface complexation modeling. *J. Colloid Interface Sci.* **2001**, *234*, 204–216.

(24) Wilkie, J. A.; Hering, J. G. Adsorption of arsenic onto hydrous ferric oxide: effects of adsorbate/adsorbent ratios and co-occurring solutes. *Colloid Surf. A* **1996**, *107*, 97–110.

(25) Vanysek, P. Electrochemical series, In *Handbook of Chemistry and Physics* 76th ed.; Lide, D. R. Ed.; CRC Press Inc: Boca Raton, Florida, 1995.

(26) Hug, S. J.; Leupin, O. Iron-catalyzed oxidation of arsenic(III) by oxygen and by hydrogen peroxide: pH-dependent formation of oxidants in the Fenton reaction. *Environ. Sci. Technol.* **2003**, *37*, 2734–2742.

(27) Manning, B. A.; Fendorf, S. E.; Goldberg, S. Surface structures and stability of arsenic(III) on goethite: Spectroscopic evidence for inner-sphere complexes. *Environ. Sci. Technol.* **1998**, *32* (16), 2383–2388.

(28) Waychunas, G. A.; Rea, B. A.; Fuller, C. C.; Davis, J. A. Surface chemistry of ferrihydrite: Part 1. EXAFS studies of the geometry of coprecipitated and adsorbed arsenate. *Geochim. Cosmochim. Acta* **1993**, *57*, 2251–2269.

(29) Waychunas, G. A.; Davis, J. A.; Fuller, C. C. Geometry of sorbed arsenate on ferrihydrite and crystalline FeOOH: re-evaluation of EXAFS results and topological factors in predicting sorbate geometry, and evidence for monodentate complexes. *Geochim. Cosmochim. Acta* **1995**, *59*, 3655–3661.

(30) Fendorf, S.; Eick, M. J.; Grossl, P.; Sparks, D. L. Arsenate and chromate retention mechanisms on goethite. 1. surface structure. *Environ. Sci. Technol.* **1997**, *31*, 315–320.

(31) Foster, A. L., Jr.; Tingle, T. N.; Parks, G. A. Quantitative arsenic speciation in mine tailings using X-ray absorption spectroscopy. *Am. Mineral.* **1998**, *83*, 553–568.

(32) Morin, G.; Lecocq, D.; Juillot, F.; Calas, G.; Ildefonse, P.; Belin, S.; Briois, V.; Dillmann, P.; Chevallier, P.; Gauthier, C.; Sole, A.; Petit, P.-E.; Borensztajn, S. EXAFS evidence of sorbed arsenic(V) and pharmacosiderite in soil overlying the Eschassières geochemical anomaly, Allier, France. *Bull. Soc. Géol. Fr.* **2002**, *173*, 281–291.

(33) Sherman, D. M.; Randall, S. R. Surface complexation of arsenic(V) to iron(III) (hydr)oxides: structural mechanism from ab initio molecular geometries and EXAFS spectroscopy. *Geochim. Cosmochim. Acta* **2003**, *67*, 4223–4230.

(34) Randall, S. R.; Sherman, D. M.; Ragnarsdottir, K. V. Sorption of As(V) on green rust ($Fe^{II}_4Fe^{III}_2(OH)_{12}SO_4 \cdot 3H_2O$) and lepidocrocite (gamma-FeOOH): surface complexes from EXAFS spectroscopy. *Geochim. Cosmochim. Acta* **2001**, *65*, 1015–1023.

(35) Catalano, J. G.; Park, C.; Zhang, Z.; Fenter, P. Simultaneous inner- and outer-sphere As(V) adsorption on α-Al_2O_3. In *Abstracts of Papers*, 231st ACS National Meeting, Atlanta, Georgia, United States, March 26–30, 2006.

ES072057S